



# Low cycle fatigue properties of friction stir welded joints of a semi-solid processed AZ91D magnesium alloy



D.R. Ni<sup>a,b</sup>, D.L. Chen<sup>a,\*</sup>, J. Yang<sup>b</sup>, Z.Y. Ma<sup>b,\*</sup>

<sup>a</sup> Department of Mechanical and Industrial Engineering, Ryerson University, 350 Victoria Street, Toronto, Ontario M5B 2K3, Canada

<sup>b</sup> Shenyang National Laboratory for Materials Science, Institute of Metal Research, Chinese Academy of Sciences, 72 Wenhua Road, Shenyang 110016, China

## ARTICLE INFO

### Article history:

Received 24 August 2013

Accepted 28 October 2013

Available online 7 November 2013

### Keywords:

Magnesium alloy

Thixomolding

Friction stir welding

Low cycle fatigue

Cyclic deformation

## ABSTRACT

A semi-solid processed (thixomolded) Mg–9Al–1Zn magnesium alloy (AZ91D) was subjected to friction stir welding (FSW), aiming at evaluating the weldability and fatigue property of the FSW joint. Microstructure analysis showed that a recrystallized fine-grained microstructure was generated in the nugget zone (NZ) after FSW. The yield strength, ultimate tensile strength, and elongation of the FSW joint were obtained to be 192 MPa, 245 MPa, and 7.6%, respectively. Low-cycle fatigue tests showed that the FSW joint had a fatigue life fairly close to that of the BM, which could be well described by the Basquin and Coffin–Manson equations. Unlike the extruded magnesium alloys, the hysteresis loops of FSW joint of the thixomolded AZ91D alloy were basically symmetrical, while the non-linear or pseudoelastic behavior was still present. The FSW joint was observed to fail in the BM section rather than in the NZ. Fatigue crack initiated basically from the pores at or near the specimen surface, and crack propagation was mainly characterized by fatigue striations along with the presence of secondary cracks.

© 2013 Elsevier Ltd. All rights reserved.

## 1. Introduction

As the lightest metallic structural materials, magnesium (Mg) alloys are promising for increasing applications in the aerospace, automobile and rail transportation industry in order to reduce the weight and improve fuel efficiency due to ever-increasing concerns about the CO<sub>2</sub> emissions and anthropogenic climate change along with highly volatile and rising energy prices [1–7]. Among them, Mg–9Al–1Zn alloy (AZ91) has increasingly been used to produce cast components due to its excellent castability and reasonable mechanical properties [8–10]. The microstructure of as-cast AZ91 alloy can be characterized by Al-lean dendrites with a eutectic Al-rich solid solution and intermetallic  $\beta$ -Mg<sub>17</sub>Al<sub>12</sub> which distributed mainly at grain boundaries with a network-like morphology [10,11]. Due to its special structure, the AZ91 castings usually exhibit unsatisfied mechanical properties, especially fatigue resistance [12–17]. Thixomolding<sup>R</sup> is a semi-solid metal processing technology for producing net-shape Mg parts in one step. This technique could provide the alloy with good mechanical properties, thereafter attracting a lot of interest and research effort [18–24].

The structural application of Mg alloys involves inevitably welding and joining during manufacturing [25–27]. However, it

is challenging to achieve defect-free welds using conventional fusion welding techniques due to the occurrence of defects such as porosity, thermal cracks, and oxidization. This hinders their development and application to some extent. Friction stir welding (FSW), as an effective solid-state joining technique, has been successfully used for welding Al and Mg alloys [28–31]. This solid-state welding technique can avoid the drawbacks of the fusion welding and produce sound joints of Mg alloys.

In the industrial applications of FSW joints, it is crucial to understand their fatigue properties which are required in determining the reliability and durability of the joints. This is also fundamental in directly influencing the structural integrity and performance of manufactured parts. However, to the authors' knowledge, no studies on the fatigue properties of FSW joints of thixomolded Mg alloys have been reported so far. In our previous study the tensile and low cycle fatigue properties of 3 mm thick thixomolded AZ91D plates without involving any welding were investigated, and this alloy was observed to exhibit good strengths and fatigue life especially at lower strain amplitudes [32,33]. It is, however, unknown how the FSW affects the fatigue life and cyclic deformation behavior of this alloy. The aim of this study was, therefore, to understand the FSW weldability and the low cycle fatigue (LCF) behavior of thixomolded AZ91D FSW joint.

\* Corresponding authors. Tel.: +1 4169795000x6487; fax: +1 4169795265 (D.L. Chen), tel./fax: +86 24 83978908 (Z.Y. Ma).

E-mail addresses: [dchen@ryerson.ca](mailto:dchen@ryerson.ca) (D.L. Chen), [zym@imr.ac.cn](mailto:zym@imr.ac.cn) (Z.Y. Ma).

## 2. Materials and methods

Thixomolded AZ91D plates with a nominal composition of 8.6Al–0.6Zn–0.26Mn (in wt.%) and a dimension of 150 mm × 100 mm × 3 mm, produced by GMAG International, were received from CANMET Materials, Natural Resources Canada, Hamilton, Ontario, Canada. The plates were subjected to FSW at a tool rotational rate of 800 rpm and a welding speed of 50 mm/min. A steel tool with a concave shoulder of 12 mm in diameter and a threaded conical pin of 4 mm in root diameter and 2.7 mm in length was adopted. The FSW was performed under the plunge control model with a tilt angle of 2.7°.

Specimens for microstructural examinations were cross sectioned perpendicular to the FSW direction. The specimens were prepared by mechanical grinding and polishing, and etched with an etching reagent consisting of 4.2 g picric acid, 10 ml acetic acid, 10 ml H<sub>2</sub>O and 70 ml ethanol. The microstructures were examined by optical microscopy (OM). Vickers hardness and tensile tests were conducted in accordance with ASTM: E384–11e1 and ASTM: E8/E8M–11, respectively. The hardness profiles were produced along the mid-thickness of the plates at an interval of 0.5 mm on the cross-section of the weld by using a computerized Buehler hardness tester under a load of 100 g for 15 s. Dog-bone-shaped tensile and fatigue specimens with a parallel section of 16 mm × 3 mm × 3 mm were machined perpendicular to the FSW direction (Fig. 1), and a gauge length of 12.5 mm was used. The specimens were electro-discharge machined and ground with SiC papers up to grit #600 to get rid of the machining marks and to achieve a smooth surface. Tensile tests were conducted at room temperature at a strain rate of  $1 \times 10^{-3} \text{ s}^{-1}$ .

Total-strain-controlled, pull-push-type LCF tests ( $R = -1$ ) were conducted in accordance with ASTM E606/E606M–12 using a computerized Instron 8801 fatigue testing system with the same specimen dimension and preparation method as those for the tensile specimens. A triangular waveform was applied at a constant strain rate of  $1 \times 10^{-2} \text{ s}^{-1}$  with strain amplitudes varying from 0.1% to 1.2%. The tests at low total strain amplitudes were operated until 10,000 cycles, after which it was changed to a load-control test at a frequency of 50 Hz. At least two specimens were tested at each strain level. Fracture surfaces were subjected to SEM examination, and some failed specimens were cut, mounted, polished to observe the area near the fracture surface via OM.

## 3. Results and discussion

### 3.1. Microstructure, microhardness, and tensile property

A sound joint of AZ91D Mg alloy was achieved after FSW, with a cap-like nugget zone (NZ) visibly formed (Fig. 2). Based on the

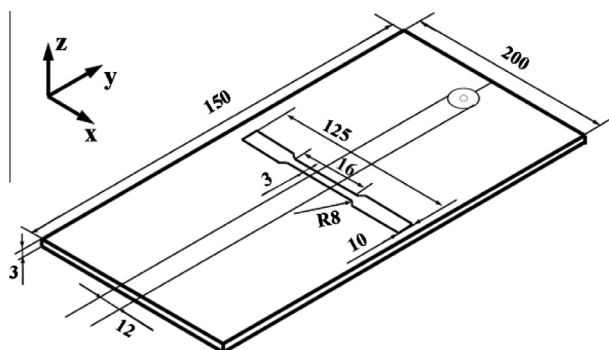


Fig. 1. Schematic illustration of FSW AZ91D plates showing fatigue specimen machining.

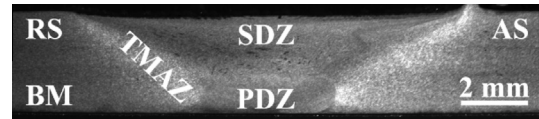


Fig. 2. Optical macrograph showing the cross-section of FSW joint of thixomolded AZ91D alloy.

microstructural characterization in the joint, three zones were obviously identified, i.e., base metal (BM), NZ, and thermomechanically-affected zone (TMAZ). The NZ could further be subdivided into two sub-zones: a large shoulder-driven zone (SDZ) and a small pin-driven zone (PDZ) [34–37].

The microstructure of the BM (Fig. 3a) consisted basically of globular primary  $\alpha$ -Mg (bright) surrounded by the network-like eutectic structure (grey) which was composed of a mixture of eutectic  $\alpha$ -Mg and intermetallic compound  $\beta$ -Mg<sub>17</sub>Al<sub>12</sub>, where the  $\beta$  particles were mainly present along the grain boundaries. Meanwhile, some Al–Mn rich particles and pores were also observed in the alloy. The microstructure of the thixomolded AZ91D Mg alloy was characterized in detail in Refs. [32,33].

The NZ was mainly characterized by fine and equiaxed grains (Fig. 3b and c). It is seen that almost no  $\beta$  particles were visible, and this was due to the fact that most of the  $\beta$  phases were broken and dissolved into the Mg matrix during FSW [10]. A typical strip-like structure containing non-uniform grains was observed in the upper SDZ (Fig. 3b), which resulted from the recrystallized structure elongated by the rotating shoulder [38]. In contrast, the lower PDZ showed more uniformly distributed equiaxed grains (Fig. 3c). The microstructures in the TMAZ were elongated along the side of the NZ and recrystallized partially (Fig. 3d).

The microhardness profile across the mid-thickness of the FSW joint is shown in Fig. 4. The hardness distribution of the BM appeared to exhibit a certain degree of fluctuation, which mainly resulted from its inhomogeneous casting microstructure with some pores (Fig. 3a). In comparison, the NZ or the center region under the shoulder had a higher hardness with a more uniform distribution. This was due to the presence of fine and equiaxed grains in the NZ (Fig. 3b and c). Based on the Hall–Petch type relationship, the smaller the grain size, the higher the microhardness [39,40].

The tensile properties of the BM and FSW joint are shown in Table 1. The yield strength (YS), ultimate tensile strength (UTS), and elongation of the BM were similar to those of the ASTM standard die cast AZ91D alloy (160 MPa, 230 MPa, and 3%) [33]. Compared to the BM, the FSW joint showed higher YS, UTS, and elongation. This was mainly attributed to the more uniformly distributed equiaxed grains (Fig. 3) and slightly higher hardness (Fig. 4) in the NZ after FSW. It should be noted that the higher tensile strengths and elongation of the FSW joint than the base metal (BM) were also related to the difference in the size of tensile samples, where the BM tensile samples had a gauge length of 25 mm (or parallel length of 32 mm) and a cross section of 6 mm × 3.2 mm (i.e., a middle parallel section volume of 614 mm<sup>3</sup>) [32,33], while the present FSW tensile samples identical to the fatigue test samples had a gauge length of 12.5 mm (or parallel length of 16 mm) and a cross section of 3.5 mm × 3.2 mm in the gauge area (i.e., a middle parallel section volume of 179 mm<sup>3</sup>). Since the thixomolded AZ91D Mg alloy still contained approximately 1.25–1.3% porosity [32,33], the larger the volume of the parallel section material was, the higher the probability of containing the shrinkage pores or other potential defects, leading to a lower ductility and strength. Indeed, it has recently been reported that both tensile ductility and strength decreased with increasing porosity and pore size in a high pressure die cast AZ91Mg alloy [41].

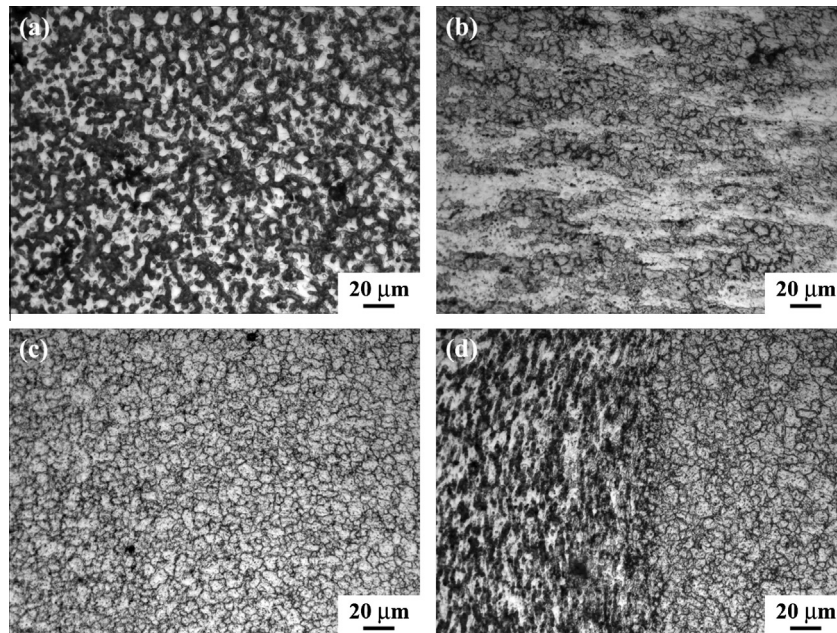


Fig. 3. Microstructures of FSW joint of thixomolded AZ91D alloy: (a) BM, (b) SDZ, (c) PDZ, and (d) TMAZ.

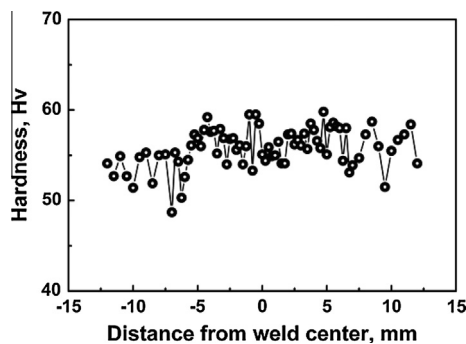


Fig. 4. Microhardness profiles of FSW joint of thixomolded AZ91D alloy along mid-thickness.

Table 1

Tensile properties of BM and FSW joint of thixomolded AZ91D alloy obtained at a strain rate of  $1 \times 10^{-2} \text{ s}^{-1}$ .

Sample <sup>a</sup>	YS (MPa)	UTS (MPa)	El. (%)
BM	162 ± 5	218 ± 8	3.3 ± 0.9
FSW joint	192 ± 3	245 ± 3	7.6 ± 1.2

<sup>a</sup> The parallel section of the tensile samples is 32 mm × 6 mm × 3.2 mm for the BM [32,33] and 16 mm × 3.5 mm × 3.2 mm for the FSW joint, respectively.

### 3.2. Cyclic deformation response

Fig. 5 shows the stress amplitude and plastic strain amplitude as a function of the number of cycles at different total strain amplitudes. As can be seen, when the total strain amplitude increased both the stress amplitude and the plastic strain amplitude increased, while the fatigue life decreased. The stress amplitude and plastic strain amplitude remained almost constant at lower strain amplitudes of 0.1% and 0.2%. At intermediate strain amplitudes (0.3–0.6%) the FSW joint underwent first slightly cyclic softening and then cyclic hardening for the remaining life. However, at higher strain amplitudes (0.8–1.2%) the FSW joint showed cyclic hardening characteristics which corresponded to decreased plastic strain amplitude until failure. These features of cyclic hardening/

softening of the FSW joint were similar to those of the BM [33], however the BM showed cyclic hardening at strain amplitudes ranging from 1.0% to 1.2% and cyclic softening ranging from 0.3% to 0.8%. This indicates that the FSW only slightly influenced the cyclic deformation behavior of the thixomolded AZ91 alloy.

The phenomena of cyclic hardening occurred at higher strain amplitudes and cyclic softening occurred at lower ones in both the BM and FSW joint were similar to those observed in an extruded AM50 alloy where cyclic hardening occurred at total strain amplitudes ranging from 0.8% to 1.5% and cyclic softening followed by hardening occurred at lower total strain amplitudes ranging from 0.4% to 0.65% [42,43]. Furthermore, Xu et al. [44] observed cyclic hardening effect in the fine grained HPDC (high pressure die cast) AM50, AE44, AJ62A alloys and cyclic softening effect in the coarse grained LPDC (low pressure die cast) AM50 alloy. Considering the fine grains in the NZ, this may explain the higher tendency of cyclic hardening of the FSW joint compared to the BM. On the other hand, it was reported that only cyclic hardening was observed at total strain amplitudes ranging 0.3–1.0% in a conventional die cast AZ91 alloy [45] and at strain amplitudes ranging 0.25–1.5% in a HPDC AZ91 alloy [46].

Patel et al. [33] considered that the cyclic hardening resulted mainly from the increase of the dislocation density during microplastic deformation and interactions between dislocations and precipitates including  $\beta$ -Mg<sub>17</sub>Al<sub>12</sub> and Al–Mn particles, as well as twin–dislocation interactions in some larger grains. For the AZ91D alloy, the hardening effect from the precipitates seemed to be more significant at the high strain levels, while the cyclic softening at the lower strain amplitudes was probably associated with dislocation annihilation and rearrangement. Meanwhile, twinning played an important role in plastic deformation of magnesium alloys [47–49]. The formation of twins during deformation can cause strain hardening or softening, depending on factors such as grain size and material crystal structure.

### 3.3. Hysteresis loops

Typical hysteresis loops for the first and mid-life cycles at a strain amplitude of 1.0% for the BM and FSW joint are shown in

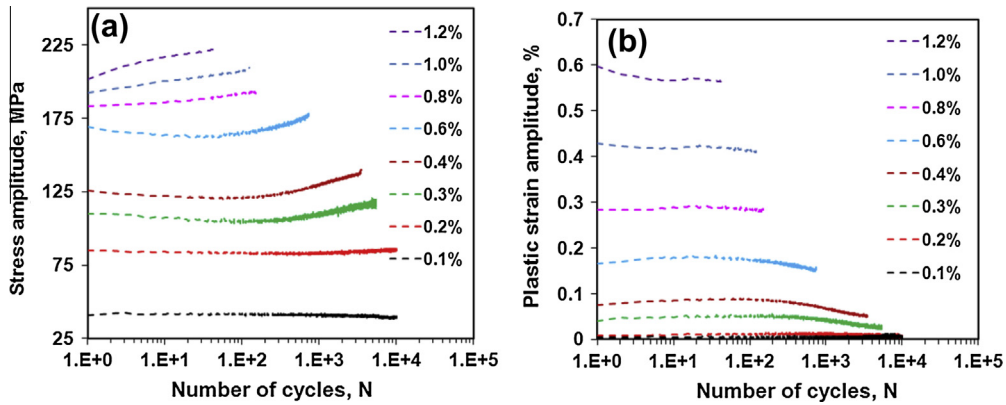


Fig. 5. (a) Stress amplitude and (b) plastic strain amplitude vs. the number of cycles at different total strain amplitudes.

Fig. 6a. It is seen that the hysteresis loops did not change much after FSW, therefore FSW did not show an apparent effect at this strain level. However, for the FSW joint, the mid-life loop showed a little cyclic hardening compared to the first-cycle loop which corresponded well to Fig. 5, while the BM did not show such a visible tendency. It can also be seen that for both the BM and FSW joint, the mid-life loop showed a slight concavity in both the ascending and descending phases, and the linear unloading portions immediately after the reversal points were quite small, which were replaced by the majority of non-linear change. Such a non-linear characteristics were mainly attributed to twinning which was discussed in detail in Ref. [33].

The mid-life hysteresis loops of the FSW joint at various total strain amplitudes are shown in Fig. 6b. At the lower strain levels (0.1% and 0.2%) the compressive stress was essentially the same as the tensile stress. At higher strain amplitudes, nearly symmetrical hysteresis loops under cyclic loading–unloading were observed, and the loops became bigger in both height and width with increasing total strain amplitude, showing a clockwise rotation. Similar loops were reported in the BM [33], as well as the other die cast AZ91 and Mg–Zn alloys [50,51]. The hysteresis loops were basically symmetrical in both the BM and FSW joint of the thixo-molded AZ91D alloy, in contrast with those of extruded Mg alloys (e.g., AM30, AZ31, and ZK60) where the hysteresis loops appeared strongly asymmetrical/skewed when the cyclic loading was applied in the extrusion direction [47–49,52–54].

3.4. Change of elastic modulus during cyclic deformation

The moduli of elasticity of the FSW joint during the loading/ascending and unloading/descending phases are shown in Fig. 7. It is seen that the increase in the total strain amplitudes led to a

decrease in the initial modulus in both loading and unloading phases, and both loading and unloading moduli showed a similar trend. At lower strain amplitudes (0.1% and 0.2%) both the moduli remained constant throughout the entire fatigue process within the experimental scatter, which was in agreement with the constant stress amplitude shown in Fig. 5a. At intermediate strain amplitudes (0.3–0.6%), both the moduli changed little for initial cycles then increased. At higher strain amplitudes (0.8–1.2%) both the moduli kept increasing monotonically in the whole cyclic deformation process, and the increasing tendency became more visible with increasing total strain amplitude. It is noticed that the changing features of the loading and unloading moduli of FSW joint during cyclic deformation were generally similar to those of the BM [33].

The magnitude of the non-linear or pseudoelastic effect in the FSW joint was associated with the applied strain amplitude, as also reported in [47]. Because the entire fatigue life at the low total strain amplitude (0.1%) was predominantly controlled by the elastic strain, the moduli obtained here were thus constant in the entire fatigue process. As the total strain amplitude increased the plastic strain amplitude also increased (Fig. 5b), and this reduced the moduli more significantly (Fig. 7). At high total strain amplitudes the plastic strain amplitude in the initial cycles was large; as it decreased during cyclic deformation (Fig. 5b), the elastic strain amplitude (the other part of the total strain amplitude) increased and the stress amplitude also increased due to the hardening effect (Fig. 5a).

3.5. Fatigue life and fatigue parameters

The total strain amplitude vs. the number of cycles to failure for the BM and FSW joint is shown in Fig. 8. Both the BM and FSW joint

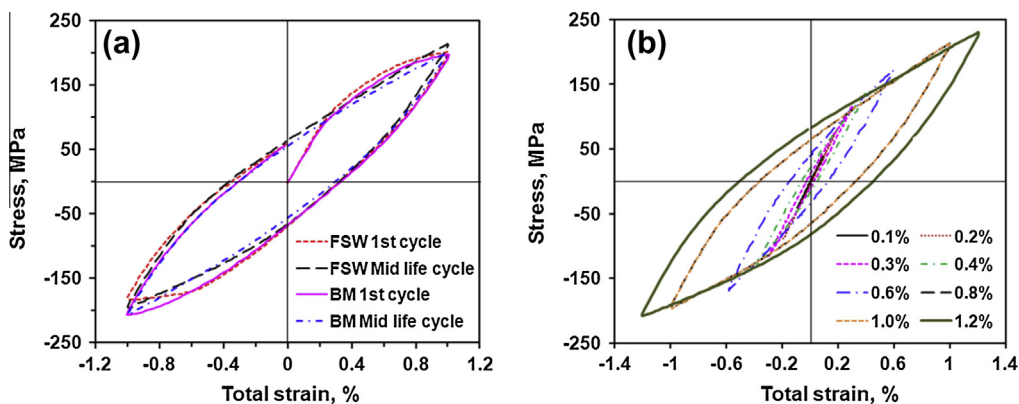


Fig. 6. Typical hysteresis loops of (a) FSW joint and BM at a total strain amplitude of 1.0% and (b) the mid-life cycles of the FSW joint at different total strain amplitudes.

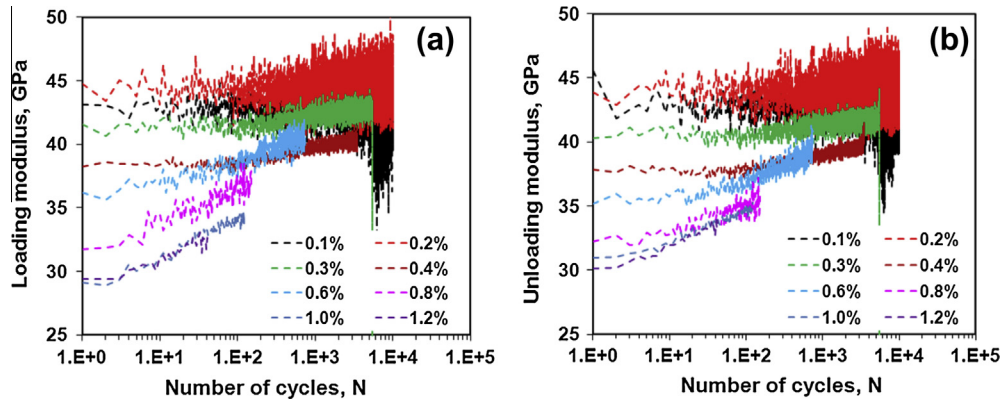


Fig. 7. (a) Loading modulus and (b) unloading modulus vs. the number of cycles at different total strain amplitudes.

showed a rising fatigue life with decreasing strain amplitude. Although the FSW joint showed a shorter fatigue life with a relatively larger experimental scatter compared to the BM at the strain amplitude of 0.2–1.2%, no failure occurred at a strain amplitude of 0.1% for both the BM and FSW joint.

Based on the Basquin and Coffin-Manson relations [33,47,48], the total strain amplitude of  $\Delta\epsilon_t/2$  consisted of elastic strain amplitude of  $\Delta\epsilon_e/2$  and plastic strain amplitude of  $\Delta\epsilon_p/2$ , which could be expressed by the following equation:

$$\frac{\Delta\epsilon_t}{2} = \frac{\Delta\epsilon_e}{2} + \frac{\Delta\epsilon_p}{2} = \frac{\sigma_f'(2N_f)^b}{E} + \epsilon_f'(2N_f)^c, \quad (1)$$

where  $E$  is the Young's modulus,  $N_f$  is the fatigue life or number of cycles to failure (or  $2N_f$  is the number of reversals to failure),  $\sigma_f'$  is the fatigue strength coefficient,  $b$  is the fatigue strength exponent,  $\epsilon_f'$  is the fatigue ductility coefficient, and  $c$  is the fatigue ductility exponent. Fig. 9 shows the total, elastic, and plastic strain amplitudes at the mid-life cycles vs. the number of reversals to failure of the BM and FSW joint. The results of both the BM and FSW joint are in good agreement and followed both the Coffin-Manson and Basquin's relationships well.

The cyclic hardening/softening behavior of fatigued materials was mainly dependent on the plastic strain amplitude, and thus the cyclic stress-strain curve could be described by the following equation [33,47,48]:

$$\frac{\Delta\sigma}{2} = K' \left( \frac{\Delta\epsilon_p}{2} \right)^{n'}, \quad (2)$$

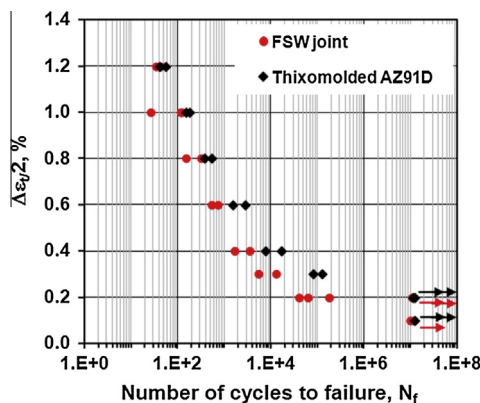


Fig. 8. Total strain amplitude as a function of the number of cycles to failure in the BM and FSW joint of the thixomolded AZ91D alloy.

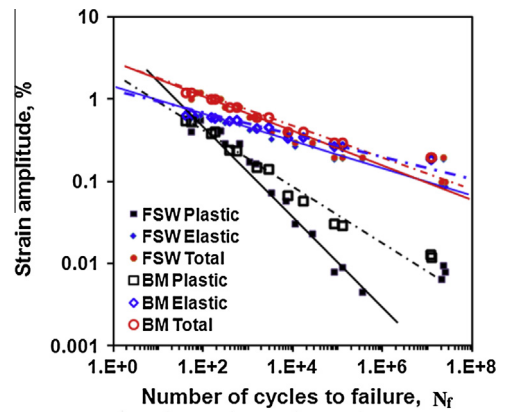


Fig. 9. Various strain amplitudes at the mid-life cycles vs. the number of reversals to failure obtained for the FSW joint and BM.

where  $K'$  is the cyclic strength coefficient,  $n'$  is the cyclic strain hardening exponent,  $\Delta\sigma/2$  and  $\Delta\epsilon_p/2$  are the stress amplitude and plastic strain amplitude of the mid-life cycle, respectively. The estimated fatigue life parameters from Eqs. (1) and (2) are summarized in Table 2. As can be seen, the cyclic strain hardening exponent  $n'$  of both the FSW joint and BM was equivalent, which was higher than their monotonic strain hardening exponent obtained at the same strain rate of  $1 \times 10^{-2} \text{ s}^{-1}$  (both  $n = 0.17$ ). This means that both of them could be hardened more significantly in the cyclic loading condition than in the monotonic loading condition.

### 3.6. Fractography

The fracture of the FSW joints was observed to occur in the parallel section of the BM randomly (not in the NZ). Fig. 10 shows typical SEM images on a fracture surface of the FSW joint fatigued at a total strain amplitude of 0.2%. Two crack initiation sites of were

Table 2

Strain-controlled fatigue parameters obtained for BM and FSW joint of thixomolded AZ91D alloy.

Low cycle fatigue parameters	FSW joint	BM
Cyclic strain hardening exponent, $n'$	0.21	0.23
Cyclic strength coefficient, $K'$ (MPa)	650	708
Fatigue strength coefficient, $\sigma_f'$ (MPa)	549	494
Fatigue strength exponent, $b$	-0.16	-0.12
Fatigue ductility coefficient, $\epsilon_f'$ (%)	0.081	0.034
Fatigue ductility exponent, $c$	-0.58	-0.39

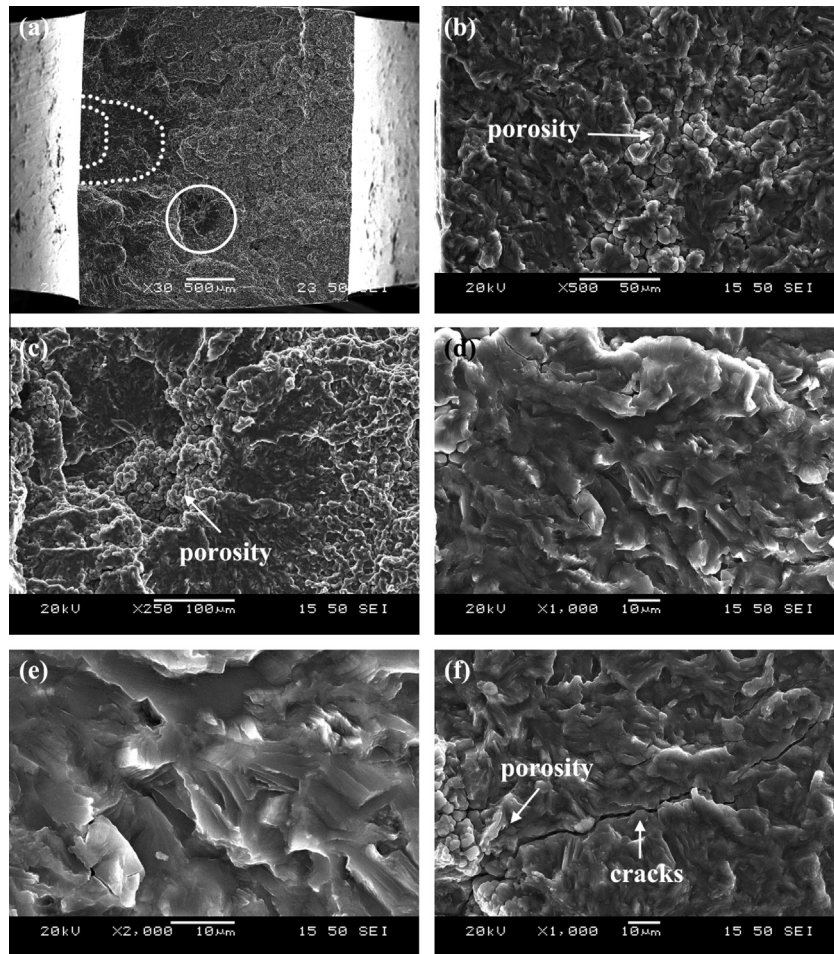


**Fig. 10.** Typical SEM fracture surface of FSW AZ91 joint fatigued at a total strain amplitude of 0.2% (failure in the BM on the RS): (a) overall view; (b) initiation site at the sample surface; (c) initiation site inside of the sample; (d) propagation zone at a lower magnification; (e) fatigue striations in the propagation zone at a higher magnification and (f) secondary cracks in the propagation zone.

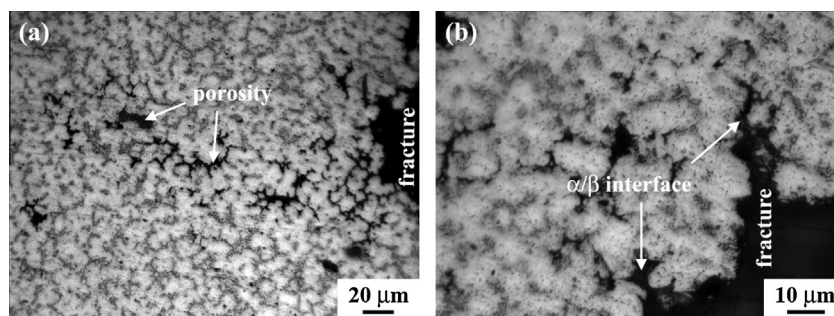


**Fig. 11.** Longitudinal cross-sectional view of failed samples near the fatigue fracture surface: (a) porosity and (b) cracks along the  $\alpha/\beta$  interface.

observed on the fracture surface (Fig. 10a). A major initiation site was located at the surface, showing that fatigue cracks initiated mainly from the specimen surface, as indicated by the dashed lines in Fig. 10a. Meanwhile, a minor one was observed inside of the sample, suggesting that the fatigue cracks could also initiate from the inside of the sample, as indicated by the solid-line circle in Fig. 10a. Further analysis showed that both the surface and inner initiation sites resulted from the pores occurred during the casting process (Fig. 10b and c). This means that although the present semi-solid thixomolded AZ91D alloy had a relatively low porosity (1.25–1.3%) and small pore size, failure still occurred due to the existence of porosity [33].

Around each initiation site there was a region of propagation zone covered with fatigue striation-like features in conjunction with tear ridges (Fig. 10d and e). This type of striations could be related to the formation of Mg twins during fatigue tests, because twins in the fatigued thixomolded AZ91D base alloy were observed in the neighborhood of the fracture surface of fatigued samples in our previous study [33]. It was also reported that the generation of twins in the plastic zone ahead of the crack tip would participate in the formation of fatigue striations in Mg alloys [24,47–49,52,53,55–57].

Some secondary cracks were observed on the fracture surface as well (Fig. 10f), which initiated from the porosity site and

crossed the propagation zone. These secondary cracks are expected to accelerate the crack propagation. Patel et al. [33] reported that in the thixomolded AZ91D BM the main fracture path occurred predominantly through the eutectic structure or grain boundary, while the secondary cracks near the fracture surface after a certain depth would also follow a similar path. Fig. 11 shows a cross-sectional view of the fatigued specimens near the fracture surface. It can be seen that fatigue cracks tended to nucleate and grow in the pores in the BM (Fig. 11a). Furthermore, the cracks were more likely to propagate along the  $\alpha/\beta$  interface or grain boundary (Fig. 11b), which confirmed the results reported by Patel et al. [33].

Cavaliere and De Marco [13] reported that friction stir processing (FSP) improved the fatigue properties of HPDC AZ91 alloy, and the enhancement was attributed to the grain refinement and especially the elimination of casting defects. Ni et al. [17] pointed out that fatigue cracks occurred preferentially within the coarse  $\beta$  particles in an as-cast AZ91D sample, but this phenomenon did not occur in the FSP sample due to the microstructure modification. Similarly, in the present study the NZ showed fine and homogeneous grain structures without network-like  $\beta$  particles and casting pores, and these features could effectively inhibit the initiation and propagation of fatigue cracks. Therefore, the FSW joint showed fairly good fatigue properties with failure occurred in the BM section rather than in the NZ.

#### 4. Conclusions

Strain-controlled low cycle fatigue tests were carried out on a thixomolded AZ91Mg alloy, and cyclic deformation characteristics, fatigue parameters and fracture behavior of the alloy were evaluated. The following conclusions can be drawn:

1. A sound FSW joint of thixomolded AZ91D Mg alloy was achieved. FSW generated a recrystallized fine-grained microstructure in the NZ. The initial coarse  $\beta$ -Mg<sub>17</sub>Al<sub>12</sub> particles in the BM were solid dissolved or broken up into fine particles, and the casting pores were eliminated as well.
2. The FSW AZ91D joint showed excellent strengths and elongation, with the YS, UTS, and elongation of 192 MPa, 245 MPa, and 7.6%, respectively. The weld showed a more uniform hardness distribution, with the NZ exhibiting the higher and more uniform hardness values.
3. Low cycle fatigue tests showed that while the FSW joint showed a shorter fatigue life than the BM at higher strain amplitudes, no failure occurred at the low strain amplitude of 0.1% for both the BM and FSW joint. Meanwhile, for both the BM and the FSW joint, the relation of elastic and plastic strain amplitudes with the number of reversals to failure showed a monotonic linear behavior and thus the Basquin and Coffin-Manson equations were well followed.
4. For both the BM and FSW joint, the cyclic hardening occurred at higher strain amplitudes but the cyclic softening occurred at lower strain amplitudes during fatigue testing. Meanwhile, no obvious change in the shape of hysteresis loops was observed after FSW.
5. Compared with the BM, the FSW joint showed a similar cyclic strain hardening exponent ( $n'$ , 0.21 vs. 0.23), which was higher than their monotonic strain hardening exponent obtained at the same strain rate (both  $n = 0.17$ ).
6. The fatigue samples of the FSW joint fractured in the BM on either the AS or RS rather than in the NZ. Both the surface and inner crack initiation sites were observed around the pores generated during the casting process, and crack prop-

agation was mainly characterized by fatigue striations with secondary cracks mainly along the  $\alpha/\beta$  interface or grain boundary.

#### Acknowledgements

This work was supported by the Natural Sciences and Engineering Research Council of Canada (NSERC) in the form of international research collaboration and the National R&D Program of China under Grant No. 2011BAE22B05 and the National Natural Science Foundation of China under Grant No. 51371179. One of the authors (D.L. Chen) is also grateful for the financial support by the Premier's Research Excellence Award (PREA), NSERC-Discovery Accelerator Supplement (DAS) Award, Canada Foundation for Innovation (CFI), and Ryerson Research Chair (RRC) program. The authors thank Dr. K. Sadayappan (CANMET Materials, Natural Resources Canada, Hamilton, Ontario, Canada) for providing the test material, and Mr. Q. Li, A. Machin, J. Amankrah, and R. Churaman (Ryerson University, Toronto, Ontario, Canada) for their assistance in the experiments.

#### References

- [1] Pollock TM. Weight loss with magnesium alloys. *Science* 2010;328:986–7.
- [2] Nie JF, Zhu YM, Liu JZ, Fang XY. Periodic segregation of solute atoms in fully coherent twin boundaries. *Science* 2013;340:957–60.
- [3] Murray J, King D. Oil's tipping point has passed. *Nature* 2012;481:433–5.
- [4] McNutt M. Climate change impacts. *Science* 2013;341:435.
- [5] Ash C, Culotta E, Fahrenkamp-Uppenbrink J, Malakoff D, Smith J, Sugden A, et al. Once and future climate change. *Science* 2013;341:472–3.
- [6] Shakun JD, Clark PU, He F, Marcott SA, Mix AC, Liu ZY, et al. Global warming preceded by increasing carbon dioxide concentrations during the last deglaciation. *Nature* 2012;484:49–54.
- [7] Mirza FA, Chen DL, Li DJ, Zeng XQ. Effect of rare earth elements on deformation behavior of an extruded Mg–10Gd–3Y–0.5Zr alloy during compression. *Mater Des* 2013;46:411–8.
- [8] Jiang JF, Wang Y, Chen G, Liu J, Li YF, Luo SJ. Comparison of mechanical properties and microstructure of AZ91D alloy motorcycle wheels formed by die casting and double control forming. *Mater Des* 2012;40:541–9.
- [9] Chen TJ, Wang RQ, Ma Y, Hao Y. Grain refinement of AZ91D magnesium alloy by Al–Ti–B master alloy and its effect on mechanical properties. *Mater Des* 2012;34:637–48.
- [10] Feng AH, Ma ZY. Enhanced mechanical properties of Mg–Al–Zn cast alloy via friction stir processing. *Scr Mater* 2007;56:397–400.
- [11] Eisenmeier G, Holzwarth B, Höppl HW, Mughrabi H. Cyclic deformation and fatigue behaviour of the magnesium alloy AZ91. *Mater Sci Eng A* 2001;319–321:578–82.
- [12] Wolf B, Fleck C, Eifler D. Characterization of the fatigue behaviour of the magnesium alloy AZ91D by means of mechanical hysteresis and temperature measurements. *Int J Fatigue* 2004;26:1357–63.
- [13] Cavaliere P, De Marco PP. Fatigue behaviour of friction stir processed AZ91 magnesium alloy produced by high pressure die casting. *Mater Charact* 2007;58:226–32.
- [14] Venkateswaran P, Raman SGS, Pathaka SD, Miyashita Y, Mutoh Y. Fatigue crack growth behaviour of a die-cast magnesium alloy AZ91D. *Mater Lett* 2004;58:2525–9.
- [15] Mayer H, Papakyriacou M, Zettl B, Stanzl-Tschegg SE. Influence of porosity on the fatigue limit of die cast magnesium and aluminium alloys. *Int J Fatigue* 2003;25:245–56.
- [16] Horstemeyer MF, Yang N, Gall K, McDowell DL, Fan J, Gullett PM. High cycle fatigue of a die cast AZ91E–T4 magnesium alloy. *Acta Mater* 2004;52:1327–36.
- [17] Ni DR, Wang D, Feng AH, Yao G, Ma ZY. Enhancing the high-cycle fatigue strength of Mg–9Al–1Zn casting by friction stir processing. *Scr Mater* 2009;61:568–71.
- [18] Pasternak L, Carnahan R, Decker R, Kilbert R. In: Brown SB, Flemings MC, editors. Proceedings of the second international conference on the processing of semi-solid alloys and composites, Cambridge, MA; 1992. p. 159–69.
- [19] Czerwinski F. Size evolution of the unmelted phase during injection molding of semisolid magnesium alloys. *Scr Mater* 2003;48:327–31.
- [20] Zhang YF, Liu YB, Zhang QQ, Cao ZY, Cui XP, Wang Y. Microstructural evolution of thixomolded AZ91D magnesium alloy with process parameters variation. *Mater Sci Eng A* 2007;444:251–6.
- [21] Zhang YF, Liu YB, Cao ZY, Zhang QQ, Zhang L. Mechanical properties of thixomolded AZ91D magnesium alloy. *J Mater Process Technol* 2009;209:1375–84.

- [22] Abolhasani D, Ezatpour HR, Sajjadi SA, Abolhasani Q. Microstructure and mechanical properties evolution of 6061 aluminum alloy formed by forward thixoextrusion process. *Mater Des* 2013;49:784–90.
- [23] Kapranos P, Ward PJ, Atkinson HV, Kirkwood DH. Near net shaping by semi-solid metal processing. *Mater Des* 2000;21:387–94.
- [24] Patel HA, Chen DL, Bhole SD, Sadayappan K. Low cycle fatigue behavior of a semi-solid processed AM60B magnesium alloy. *Mater Des* 2013;49:456–64.
- [25] Patel VK, Bhole SD, Chen DL. Formation of zinc interlayer texture during dissimilar ultrasonic spot welding of magnesium and high strength low alloy steel. *Mater Des* 2013;45:236–40.
- [26] Chowdhury SH, Chen DL, Bhole SD, Cao X, Wanjara P. Friction stir welded AZ31 magnesium alloy: microstructure, texture, and tensile properties. *Metall Mater Trans A* 2013;44:323–36.
- [27] Liu C, Chen DL, Bhole S, Cao X, Jahazi M. Polishing-assisted galvanic corrosion in the dissimilar friction stir welded joint of AZ31 magnesium alloy to 2024 aluminum alloy. *Mater Charact* 2009;60:370–6.
- [28] Mishra RS, Ma ZY, Charit I. Friction stir processing: a novel technique for fabrication of surface composite. *Mater Sci Eng A* 2003;341:307–10.
- [29] Ma ZY. Friction stir processing technology: a review. *Metall Mater Trans A* 2008;39A:642–58.
- [30] Mishra RS, Ma ZY. Friction stir welding and processing. *Mater Sci Eng R* 2008;53:980–1–78.
- [31] Nandan R, DebRoy T, Bhadeshia HKDH. Recent advances in friction-stir welding-process, weldment structure and properties. *Prog Mater Sci* 2008;53:980–1023.
- [32] Patel HA, Chen DL, Bhole SD, Sadayappan K. Microstructure and tensile properties of thixomolded magnesium alloys. *J Alloys Compd* 2010;496:140–8.
- [33] Patel HA, Chen DL, Bhole SD, Sadayappan K. Cyclic deformation and twinning in a semi-solid processed AZ91D magnesium alloy. *Mater Sci Eng A* 2010;528:208–19.
- [34] Arbegast WJ. A flow-partitioned deformation zone model for defect formation during friction stir welding. *Scr Mater* 2008;58:372–6.
- [35] Zhang Z, Xiao BL, Wang D, Ma ZY. Effect of alclad layer on material flow and defect formation in friction-stir-welded 2024 aluminum alloy. *Metall Mater Trans A* 2011;42A:1717–26.
- [36] Zhang Z, Xiao BL, Ma ZY. Effect of welding parameters on microstructure and mechanical properties of friction stir welded 2219Al–T6 joints. *J Mater Sci* 2012;47:4075–86.
- [37] Zhou L, Nakata K, Liao J, Tsumura T. Microstructural characteristics and mechanical properties of non-combustive Mg–9Al–Zn–Ca magnesium alloy friction stir welded joints. *Mater Des* 2012;42:505–12.
- [38] Ni DR, Xue P, Wang D, Xiao BL, Ma ZY. Inhomogeneous microstructure and mechanical properties of friction stir processed NiAl bronze. *Mater Sci Eng A* 2009;524:119–28.
- [39] Fairman M, Afrin N, Chen DL, Cao XJ, Jahazi M. Microstructural evaluation of friction stir processed AZ31B–H24 magnesium alloy. *Can Metall Q* 2007;46:425–32.
- [40] Patel VK, Bhole SD, Chen DL. Influence of ultrasonic spot welding on microstructure in a magnesium alloy. *Scr Mater* 2011;65:911–4.
- [41] Biswas S, Sket F, Chiumenti M, Gutiérrez-Urrutia I, Molina-Aldareguía JM, Pérez-Prado MT. Relationship between the 3D porosity and  $\beta$ -phase distributions and the mechanical properties of a high pressure die cast AZ91 Mg alloy. *Metall Mater Trans A* 2013;44A:4391–403.
- [42] Chen LJ, Wang CY, Wu W, Liu Z, Stoica GM, Wu L, et al. Low-cycle fatigue behavior of an as-extruded AM50 magnesium alloy. *Metall Mater Trans A* 2007;38:2235–41.
- [43] Liu Z, Ji HT, Lin L, Chen LJ, Wu W, Yang L. Cyclic deformation behavior and potential automobile application of magnesium die casting alloys AZ91 and AM50. *Mater Sci Forum* 2007;539–543:1626–31.
- [44] Xu S, Gertsman VY, Li J, Thomson JP, Sahoo M. Role of mechanical twinning in tensile compressive yield asymmetry of die cast mg alloys. *Can Metall Q* 2005;44:155–66.
- [45] Chen LJ, Shen J, Wu W, Li F, Wang Y, Liu Z. Low-cycle fatigue behavior of magnesium alloy AZ91. *Mater Sci Forum* 2005;488–489:725–8.
- [46] Liu Z, Xu YY, Wang ZG, Wang Y, Liu ZY. Low cycle fatigue behavior of AZ91HP alloy in as high pressure die casting. *Acta Metall Sin (English Lett)* 2000;13:961–6.
- [47] Begum S, Chen DL, Xu S, Luo AA. Low cycle fatigue properties of an extruded AZ31 magnesium alloy. *Int J Fatigue* 2009;31:726–35.
- [48] Begum S, Chen DL, Xu S, Luo AA. Strain-controlled low-cycle fatigue properties of a newly developed extruded magnesium alloy. *Metall Mater Trans A* 2008;39:3014–26.
- [49] Wu L, Jain A, Brown DW, Stoica GM, Agnew SR, Clausen B, et al. Twinning-detwinning behavior during the strain-controlled low-cycle fatigue testing of a wrought magnesium alloy, ZK60A. *Acta Mater* 2008;56:688–95.
- [50] Cáceres CH, Sumitomo T, Veidt M. Pseudoelastic behaviour of cast magnesium AZ91 alloy under cyclic loading–unloading. *Acta Mater* 2003;51:6211–8.
- [51] Mann GE, Sumitomo T, Cáceres CH, Griffiths JR. Reversible plastic strain during cyclic loading–unloading of Mg and Mg–Zn alloys. *Mater Sci Eng A* 2007;456:138–46.
- [52] Lin XZ, Chen DL. Strain controlled cyclic deformation behavior of an extruded magnesium alloy. *Mater Sci Eng A* 2008;496:106–13.
- [53] Fan CL, Chen DL, Luo AA. Dependence of the distribution of deformation twins on strain amplitudes in an extruded magnesium alloy after cyclic deformation. *Mater Sci Eng A* 2009;519:38–45.
- [54] Wu L, Agnew SR, Brown DW, Stoica GM, Clausen B, Jain A, et al. Internal stress relaxation and load redistribution during the twinning–detwinning-dominated cyclic deformation of a wrought magnesium alloy, ZK60A. *Acta Mater* 2008;56:3699–707.
- [55] Begum S, Chen DL, Xu S, Luo AA. Effect of strain ratio and strain rate on low cycle fatigue behavior of AZ31 wrought magnesium alloy. *Mater Sci Eng A* 2009;517:334–43.
- [56] Patel HA, Rashidi N, Chen DL, Bhole SD, Luo AA. Cyclic deformation behavior of a super-vacuum die cast magnesium alloy. *Mater Sci Eng A* 2012;546:72–81.
- [57] Mirza FA, Chen DL, Li DJ, Zeng XQ. Low cycle fatigue of a rare-earth containing extruded magnesium alloy. *Mater Sci Eng A* 2013;575:65–73.